*Proceedings of the 10th World Congress on Mechanical, Chemical, and Material Engineering (MCM'24)*
*Barcelona, Spain –August 22-24, 2024*
*Paper No. HTFF 171*
*DOI: 10.11159/htff24.171*

# Numerical and Experimental Investigation of the Thermal Characteristics of Quartz Infrared Lambs

**Atakan Karabatak[1,2], Tamer Calisir[2]**
[1]Turkish Aerospace Industries, Inc
Fethiye Mahallesi, Havacılık Bulvarı No:17 06980 Kahramankazan Ankara, Turkey
[2]Gazi University, Graduate School of Applied and Natural Sciences, Mechanical Engineering Dept.
Ankara, Türkiye
atakan.karabatak@tai.com.tr; tamercalisir@gazi.edu.tr
[2]Gazi University, Faculty of Engineering, Mechanical Engineering Dept.
06570 Maltepe, Ankara, Türkiye

***Abstract*** **-** Examining the thermal performance of infrared (IR) lamps is very important in industrial applications to ensure that the desired heating power can be obtained in the most efficient way. Reasons such as high operating temperatures, complex geometric structures and dominant radiative heat dissipation properties make it very difficult to carry out analytical calculations about their working principles. In this article, the thermal performances of four vertically placed IR lamps were examined experimentally and numerically under different parameters. An experimental test setup (ETS) and a thermal mathematical model (TMM) were created to examine the power, distance, location of heat flux sensor (HFS) and angle parameters precisely. Many studies were examined to obtain the input parameters to be defined in the numerical model, and two equations created using the net radiation method were used to calculate the quartz and filament temperatures of IR lamps. These equations were solved numerically with a MATLAB code using the Newton-Raphson method. The TMM was validated thanks to the experimental data and the obtained input values. The average relative error rates between numerical results and experimental results were calculated as 5.1%, 3.7%, 6.4% and 3.2% for location, distance, angle and power parameters, respectively. In addition, with the help of the verified TMM, it was examined how the thermal performance of IR lamps changes in a vacuum environment and with the changing emissivity coefficient of the ceramic coated rear surface of them.

***Keywords*****:** infrared quartz lamb, thermal performance, radiative heat flux, radiant heat flux sensor

## 1. Introduction

IR heating elements have various application areas such as space simulation of solar and Earth's surface heat fluxes for qualification tests of spacecraft, as well as heating in both open and enclosed spaces, and in industrial processes requiring high levels of heat. Depending on the wavelength of the emitted heat, quartz IR heaters are categorized into three types: short-wave, medium-wave, and long-wave IR heaters. As the temperature increases, the wavelength becomes shorter, and the intensity of IR radiation becomes higher [1]. As a type of IR heaters, quartz IR lamps emit IR rays with wavelengths ranging from 0.7 to 1.4 μm and they can reach maximum temperatures within a few seconds, up to power densities of 130 $kW.m^{-2}$ or higher [2]. A picture of a quartz IR lamp, a schematic representation of the electrical circuit of a quartz IR lamp and description of its components are given in Fig. 1. Essentially, a quartz IR lamp consists of a tungsten serpentine wire that has operating temperature between 2200-2800 K, a tube made of quartz glass (with the rear surface coated with a ceramic component), and an inert gas filling the space between the serpentine wire and the quartz tube. The quartz envelope must be sealed to prevent contact between the tungsten filament and oxygen. These lamps contain either a vacuum or, more commonly, an inert atmosphere consisting of some noble gases such as nitrogen, neon, or argon [3].

When the working principles of an IR lamp are examined, it is observed that there are many factors affecting their heating performance. In this study, it is aimed to investigate numerically and experimentally the heating power provided by quartz IR lamps operated at different power levels (between 100W and 500W), against surfaces with different distances (250 mm -750 mm), coordinates (in the range of -18 cm to +18 cm along the x and y axes) and angles (ranged from -60° to +60°). In addition to power, distance, coordinates and angle parameters, numerical studies have been conducted for scenarios that IR lamps are operated in a vacuum environment and have ceramic coated rear surfaces with different emission values.

Brown et al. [4] calculated the efficiency of an industrial ceramic infrared heater by increasing its power up to 600 W and obtained a heat flux map in a volume of 500mm x 500mm x 500mm in front of the heater. As a similar study, Butturini

and Ngo [5] produced the heat flux distribution of 4 different types of infrared heaters on a plane (along the x and y axis) with measurements taken from the heaters with the help of a liquid-cooled heat flux sensor. Er et al. [6] confirmed the TMM with the help of measurements taken by moving a heat flux sensor at a fixed distance along a single axis for different power values of a horizontally placed IR lamp. It is observed that there was a maximum difference of 6.3% between TMM results and experimental data.

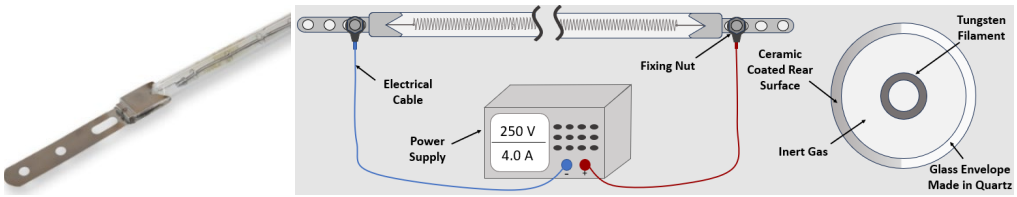


Fig. 1: (a) Picture of Quartz IR Lamp, (b) Schematic Representation of Quartz IR Lamp [7]

In this study, both experimental and numerical methods have been employed with the help of the designed ETS and created TMM. Numerical calculations were performed using the Steady State Thermal module of ANSYS software. The measurement results were compared with the solved TMM results to validate the TMM. After validation, TMM was modified and solved for scenarios where the IR lamps operated in a vacuum environment and had ceramic-coated rear surfaces with emissivity values (ε) of 0.3, 0.5 and 0.7. Unlike the studies in the literature, detailed information was obtained regarding the thermal performance of multiple quartz IR lamps placed vertically in a controlled volume under 4 different parameters. Thanks to TMM verified with the data obtained, it is aimed to speed up the numerical studies to be carried out in future studies by reducing the effort and time spent on experimental studies.

## 2. Experimental Studies

### 2.1. ETS and Auxiliary Equipment

The experimental studies were carried out in a thermal vacuum test system (TVTS) located in an ISO-8 class clean room, which provides a temperature and humidity-controlled environment. The ETS consists of a sigma profile structure that holds the whole structure together, four vertically placed IR heater lamps, the HFS that can be moved separately in axes to measure the heat flux and test cabling. The IR lamps located on the ETS are connected to separate power supplies. An illustration and the view of ETS that located in TVTS and is given in Fig. 2(b) and Fig. 2(c) respectively.

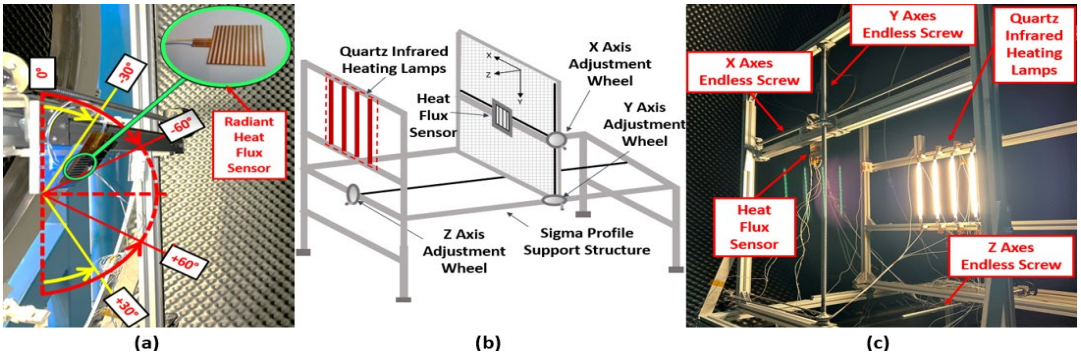


Fig. 2: An Illustration and the View of ETS that Located in TVTS and Angular Layout of the HFS

The ETS was designed to allow the HFS to move independently in two axes (x and y axis) and the frame to which the IR lamps are attached to move in one axis (z axis). To provide movement in these three axes, an endless screw and nut connection is used to convert rotational motion to linear motion. To obtain the measurements of the HFS at different angles,

two parts that have different internal angles were designed. These parts were printed with a 3D printer using PLA filament. With these parts, the HFS was placed on the ETS with -30°, -60°, +60° and +30° angles. The angles where the HFS was placed and the view of HFS is shown in Fig. 2(a). The HFS that was shown in Fig. 2(a) used during heat flux measurements is a standard radiant HFS manufactured by CAPTEC. The dimensions of this HFS are 30 mm x 30 mm, the sensitivity value is 4.9 μV/W/m$^2$ and the operating temperature range is -200 / +250 °C [8]. To calculate the net heat flux value, the voltage value of μV read on the HFS is divided by the sensitivity value of the HFS. To measure the temperature of the HFS, it is sufficient to define the channels which the sensor is connected as a T-type thermocouple (TC) in data acquisition system (DAS). During the heat flux measurement activities, the door of the TVTS was closed to prevent the clean room air conditioning system from creating forced convection able to effect on the ETS. To observe the temperature distribution (ambient temperature) around the ETS, TCs were located on the thermal shroud structure that surrounds inside of the TVTS.

### 2.2. Experimental Measurements

Before starting the heat flux measurements, to observe the time-dependent change in the heat flux emitted by the four IR lamps, the HFS was located at x=0, y=0 positions and the distance on the z axis that 500 mm away from the IR lamps. As a result of these measurements, it was observed that the measured heat flux value became constant approximately 1 hour after the measurement started. Based on this information, during the experimental studies, the measurements were started after 1 hour. The graph of the data collected during this measurement is shown in Fig. 3.

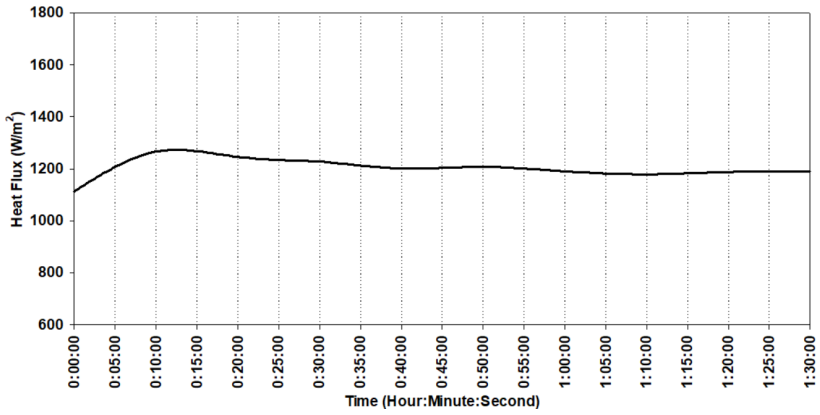


Fig. 3: Time-dependent Heat Flux Measurement of IR Lamps

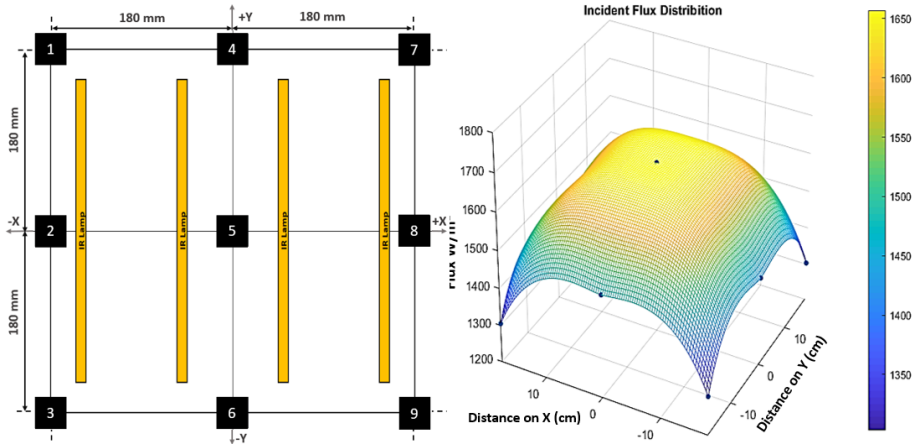


Fig. 4: HFS Measurement Points and the Graph of Heat Flux Data

The first heat flux measurement aimed to measuring heat flux distribution in front of the IR lamps along x and y axes. To obtain the heat flux distribution, 9 measurement points have been specified. 8 of these 9 points were located on edges of a square plane with dimensions of 360 mm x 360 mm and the last point was located at the center of this plane. The layout of these 9 measurement points and collected heat flux data are represented in Fig. 4. During these measurements, the angle of the HFS was set to zero degrees, the electrical power supplied to each of the IR lamps was set to 500 W and the distance on the z axis between the HFS and the IR lamps was set to 500 mm.

Afterwards, the effect of the distance between the HFS and IR lamps on the measured heat flux value was examined. For this purpose, the distance between the IR lamps and the HFS (on the z-axis) was adjusted to 250 mm, 500 mm and 750 mm and heat flux data were collected at these points. During these measurements, the angle of the HFS was set to zero degrees and the electrical power supplied to each of the IR lamp was set to 500 W. Experimental studies continued with measurements where the HFS was placed at different angles in front of the IR lamps. During these measurements, the angle of the HFS was adjusted to +60, -60, +30 and -30 degrees that were shown in Fig. 2, and heat flux data were collected at these angles. Along these measurements, the electrical power supplied to each of the IR lamp was set to 500 W and the distance on the z-axis between the HFS and the IR lamps was set to 500 mm. Final experimental studies were done to measure the heat flux values according to different electrical power inputs of IR lamps. The electrical power values were set to 100, 300 and 500 W, respectively, and heat flux data were collected at these power levels. During these measurements, the angle of the HFS was set to zero degrees and the distance on the z-axis between the HFS and the IR lamps was set to 500 mm.

## 3. Numerical Studies

### 3.1. Net Radiation Method

Er et al. [6] calculated that the temperatures of the tungsten filament and quartz glass envelope in a 500 W powered IR lamp, and showed that the temperature values can reach 2189 K and 859 K, respectively. Experimental measurement of these temperatures is very difficult due to geometrical limitations and difficulty of finding suitable measurement equipment. In order to obtain these temperatures, Er et al. [6] and Schmidt et al. [9] used two equations that are called net radiation method. These equations and descriptions of the variables are as follows.

$$P\eta - \varepsilon_f(T_f) S_f \sigma {T_f}^4 - 2\pi L_q k_{Argon}(T^*) \frac{T_f - T_Q}{\ln\left(\frac{d_Q}{d_f}\right)} = 0 \tag{1}$$

$$\alpha_Q \varepsilon_f(T_f) S_f \sigma {T_f}^4 + 2\pi L_q k_{Argon}(T^*) \frac{T_f - T_Q}{\ln\left(\frac{d_Q}{d_f}\right)} - \varepsilon_Q S_Q \sigma {T_Q}^4 - h S_Q (T_Q - T_\infty) = 0 \tag{2}$$

P: Applied power to the IR lamp
$\varepsilon_f$: Filament Emissivity
$T_f$: Filament Temperature
$S_f$: Filament Surface Area
$S_Q$: Quartz Surface Area
$\alpha_Q$:Quartz Absorbtivity
$k$: Argon Conductivity
$\eta$: Lamp Efficiency
$T^*$: Mean Temperature
$T_Q$: Quartz Temperature
$d_Q$: Quartz Diameter
$d_f$: Filament Diameter
$L_q$: Length of Quartz
h: Heat Transfer Coef.
$\varepsilon_Q$: Quartz Emissivity

Eqs. (1) - (2) were solved with a MATLAB code generated using the Newton-Raphson method. The filament temperature ($T_f$) and quartz temperature ($T_Q$) were calculated according to power inputs of the IR lamp. Parameters that were used to calculate $T_f$ and $T_Q$ temperature values are listed in Table 1. As stated in the user manual [10] of the PHILIPS brand 13195X/98 model IR lamps that are used in this study, more than 85% of the consumed energy is transmitted into IR heat in IR lamp. Therefore, the efficiency (η) of IR lamps was chosen as 85% for all power values. Kuntze and Ghidersa [11] and Er et al. [6] showed an analysis of the IR lamp for a quartz emissivity ($\varepsilon_Q$) of 0.90. Based on this information, $\varepsilon_Q$value was accepted as 0.90 for all power values. Forsythe et al. [12] gave the total emissivity value in a graph for a certain temperature range (1100K-3700K) in their study. These values listed in study of Er et al. [6] are shown in Table 2.

Table 1: Net Radiation Equations Parameters

| Parameter | 100W Power Input | 300W Power Input | 500W Power Input |
|---|---|---|---|
| P (W) | 100 | 300 | 500 |
| $\eta$ | 0.85 | 0.85 | 0.85 |
| $\varepsilon_f$ | 0.1885 | 0.2487 | 0.273 |
| $\varepsilon_Q$ | 0.9 | 0.9 | 0.9 |
| $d_Q$(m) | $1.1\text{x}10^{-2}$ | $1.1\text{x}10^{-2}$ | $1.1\text{x}10^{-2}$ |
| $S_f$ ($m^2$) | $1.18\text{x}10^{-3}$ | $1.18\text{x}10^{-3}$ | $1.18\text{x}10^{-3}$ |
| $d_f$ (m) | $2.4\text{x}10^{-4}$ | $2.4\text{x}10^{-4}$ | $2.4\text{x}10^{-4}$ |
| $S_Q$($m^2$) | $5.1\text{x}10^{-3}$ | $5.1\text{x}10^{-3}$ | $5.1\text{x}10^{-3}$ |
| $L_q$(m) | 0.295 | 0.295 | 0.295 |
| $\alpha_Q$ | 0.9 | 0.9 | 0.9 |
| h($W/m^2K$) | 11.2 | 11.2 | 11.2 |
| $k$(mW/m.K) | 55 | 55 | 55 |

Table 2: Variation of Tungsten Emissivity with Temperature [6]

| Temperature (K) | Total Emissivity |
|---|---|
| 1500 | 0.192 |
| 1800 | 0.236 |
| 2000 | 0.259 |
| 2200 | 0.278 |

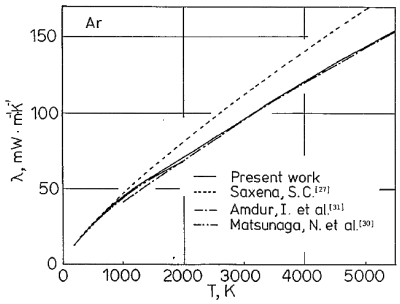


Fig. 5: Thermal Conductivity of Argon at High Temperatures [13]

The filament emissivity value ($\varepsilon_f$) was obtained by interpolating according to the calculated filament temperature. The values of $d_Q$, $S_f$, $d_f$, $S_Q$ and $L_q$ variables that were calculated and measured in the study of Er et al. [6]. The convection heat transfer coefficient (h), it has been seen that h value on the surface of a vertically placed cylindrical object that has the same geometric properties as the IR lamp has been obtained by performing a CFD analysis. Therefore, a cylindrical object with the same geometric features as the IR lamp was placed in a large control volume and the numerical model was calculated. The surface temperature of the IR lamp was assumed 2189K. The calculated convection heat transfer value was divided by the surface area of the IR lamp and the value of convection coefficient was found 11.2 $W/m^2K$. In the study of Er et al. [6], it was seen that the difference between the h values used for the 250W, 500W and 750W values of the IR lamp was quite small, so the h value was accepted as the same for all power values. Hoshino et al. [13] measured the thermal conductivity of high purity argon gas in their study. Hoshino et al. [13] executed these measurements by taking 37 measurements in the temperature range of 300K - 4500K and presented them with a graph comparing them with similar studies (Fig. 5). As it is

known from the work of Er et al. [6], the mean temperature ($T^*$) inside an IR lamp that is powered with 500 W is around 1500K. Thermal conductivity corresponding to 1500K in Fig. 5 is 55 mW/mK. Since it was seen that this value is not varying much at 1000K, the thermal conductivity value of argon was accepted as 55 mW/m.K for all power values.

### 3.2. Thermal Mathematical Model

The thermal analysis was conducted using the Steady State Thermal module in the ANSYS V19.2 Software, a commercial software renowned for thermal analysis. In the TMM, the tungsten filament was simplified as a cylinder instead of its actual helical structure for geometric simplicity. Only half of the quartz tube was modelled to simulate the ceramic-coated back surface. Other components of the ETS were omitted due to their negligible thermal conductivity. A thin square plate represented the HFS in the model. Surface-to-surface radiation method was used, with surface properties and temperatures of components determined both theoretically and experimentally as inputs into the model. Radiative parameters such as incoming, emitted, and net radiation were obtained using radiation probe tool within the software. TMM and variables that were implemented in the model are shown in Fig. 6.

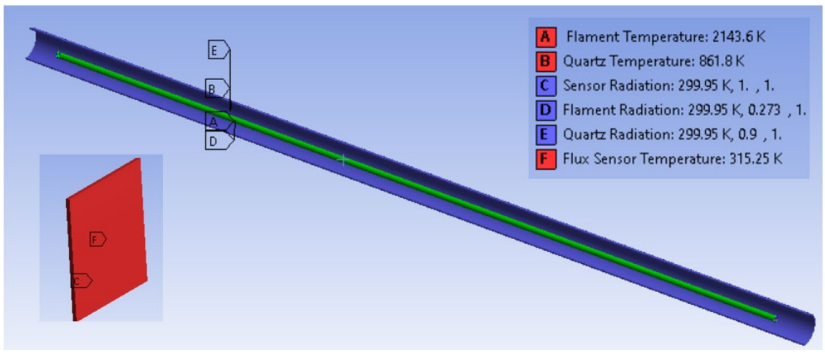


Fig. 6: TMM and the Input Variables

## 4. Results

The experimental heat flux measurements executed to obtain the heat flux distribution in front of the IR lamps along the x and y axes compared with the TMM results and plotted in Fig. 7(a). Also, obtained experimental data, numerical results and relative errors are shown in Table 3.

Table 3: TMM, Experimental Results and Relative Errors for the Heat Flux Distribution in Front of the IR Lamps

| Measurement Point | Distance on X Axis (mm) | Distance on Y Axis (mm) | Temp. of HFS (K) | Ambient Temp. (K) | Exp. Heat Flux (W/m2) | TMM Heat Flux (W/m2) | Rel. Err. (%) |
|---|---|---|---|---|---|---|---|
| **1** | -180 | +180 | 312.15 | 299.45 | 1269.7 | 1305.3 | 2.8 |
| **2** | -180 | 0 | 312.65 | 299.45 | 1395.4 | 1475.1 | 5.7 |
| **3** | -180 | -180 | 313.45 | 299.95 | 1221.3 | 1304.0 | 6.8 |
| **4** | 0 | +180 | 314.65 | 299.95 | 1407.5 | 1450.6 | 3.1 |
| **5** | 0 | 0 | 315.25 | 299.95 | 1559.0 | 1651.2 | 5.9 |
| **6** | 0 | -180 | 313.95 | 299.95 | 1343.3 | 1435.1 | 6.8 |
| **7** | +180 | +180 | 312.55 | 299.45 | 1285.9 | 1308.1 | 1.7 |
| **8** | +180 | 0 | 314.15 | 299.45 | 1397.0 | 1485.1 | 6.3 |
| **9** | +180 | -180 | 312.95 | 299.45 | 1224.9 | 1303.2 | 6.4 |

In Fig. 7, the experimental heat flux measurements taken for the different distance values between the HFS and IR lamps (Fig. 7b), the different angle orientations of the HFS (Fig. 7c) and the different power values (Fig. 7d) compared with the TMM results and plotted. Also, the experimental data, numerical results and relative errors for all these scenarios are shown in Table 4. In addition to the numerical studies that are mentioned above, the TMM model was used to calculate the heat

flux values if the ETS was in vacuum condition and the emissivity of the ceramic coating on IR lamps rear surface was 0.3, 0.5 and 0.7 when HFS located at meas. point five that is shown in Fig. 4 and 500mm far from IR lamps for 500W power distribution. The heat flux value calculated for vacuum condition has been obtained as 1810.9 W/m$^2$ and the heat flux values calculated for the 0.3, 0.5 and 0.7 emissivity values of ceramic coating have been obtained as 1989.1, 1842.8 and 1734.6 W/m$^2$, respectively.

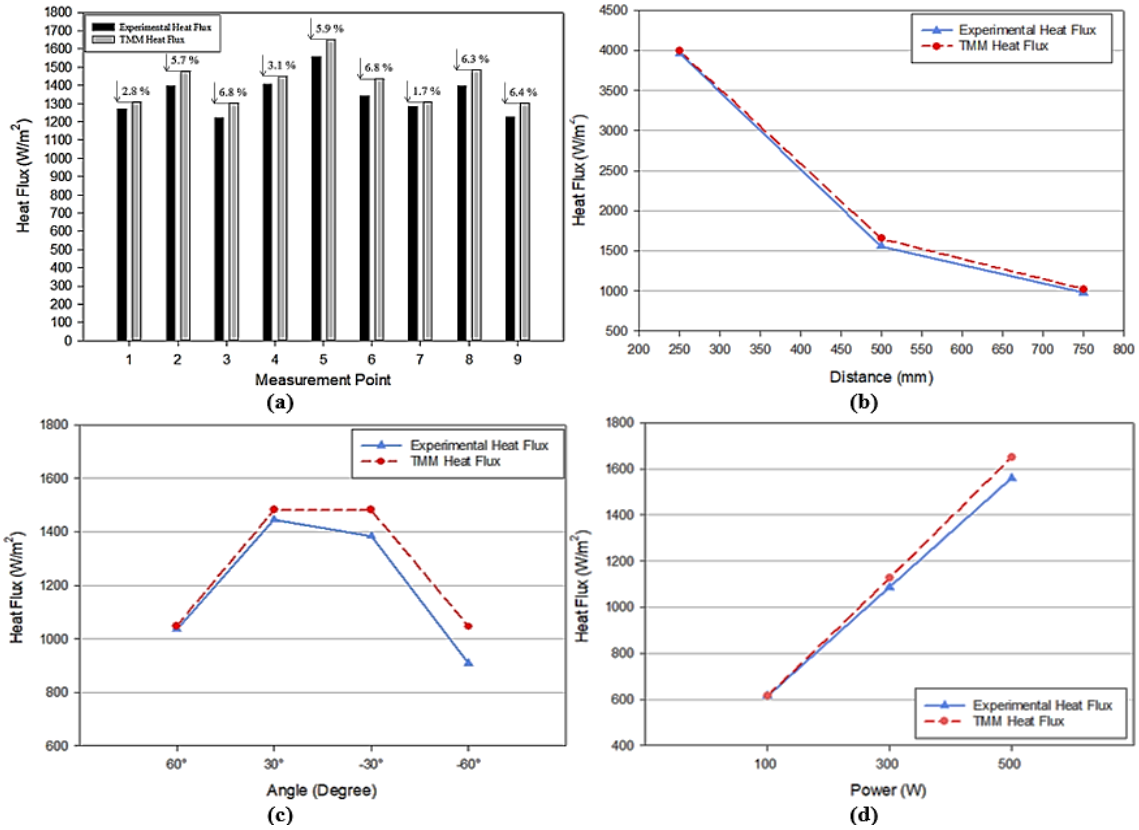


Fig. 7: Comparison of TMM and Experimental Heat Flux Results

Table 4: TMM Results, Collected Experimental Data and Relative Errors

| Distance (mm) | Temp. of HFS (K) | Ambient Temp. (K) | Exp. Heat Flux (W/m2) | TMM Heat Flux (W/m2) | Rel. Err. (%) |
|---|---|---|---|---|---|
| 250 | 344.25 | 298.5 | 3966.3 | 3992.44 | 0.7 |
| 500 | 315.25 | 299.95 | 1559 | 1651.22 | 5.9 |
| 750 | 305.75 | 299.05 | 979.2 | 1023.37 | 4.5 |
| **The Angle of the HFS (Degree)** | | | | | |
| 60° | 316.85 | 298.85 | 1037.3 | 1048.86 | 1.1 |
| 30° | 316.15 | 298.85 | 1446.2 | 1482.44 | 2.5 |
| -30° | 318.85 | 298.38 | 1384.6 | 1481.56 | 7.0 |
| -60° | 319.75 | 299.1 | 909 | 1045.78 | 15.0 |
| **Power of the IR Lamp (W)** | | | | | |
| 100 | 299.35 | 295.35 | 615.3 | 614.4 | 0.1 |
| 300 | 309.05 | 295.35 | 1087 | 1125.4 | 3.5 |
| 500 | 315.25 | 299.95 | 1559 | 1651.22 | 5.9 |

## 4. Conclusion

In this study, numerical and experimental studies were carried out on the parameters affecting the heating effect of IR lamps and thus TMM was verified. It was observed that the relative error between the measurements made on the x and y axis and the TMM results against IR lamps was between 1.7% and 6.8%, and the average of all errors was only 5.1%. When the studies conducted for different distance values on the Z axis were examined, it was seen that as the distance got shorter, the relative error between them decreased and reached a very low error rate of 0.7%. When the relative error between the studies on the angle values of HFS were examined, it was seen that the error rates were quite low in positive angles and high in negative angles. It was concluded that this is since although the IR lamps are defined with a homogeneous temperature on the TMM, the bottom side of the IR lamps is colder than the upper side due to the natural convection occurs around the IR lambs and the HFS faces the cold bottom side of the IR lamps, especially at negative angles. The studies carried out for different power values of IR lamps, it was seen that the relative error between TMM and experimental data was proportional to the increase in power value. In studies conducted only with TMM, it has been observed that IR lamps work more efficiently when working in a vacuum environment because they do not cool down like normal conditions, but they work less efficiently when the emissivity of the ceramic coating of quartz increases.

## References


[1] S. Slavov, D. Dimitrov, and P. Zlateva, "Investigation the influence of surface topography on scattering ability of aluminium reflectors from infrared quartz heater," presented at the IOP Conference Series: Materials Science and Engineering, Oct. 2019, p. 012006. doi: 10.1088/1757-899X/564/1/012006.

[2] Z. Pan and G. G. Atungulu, *Infrared Heating for Food and Agricultural Processing*. CRC Press, 2010.

[3] M. Pettersson, "Heat Transfer and Energy Efficiency in Infrared Paper Dryers," Doctoral Thesis (compilation), Chemical Engineering, Lund University, 1999.

[4] K. J. Brown, R. Farrelly, S. M. O'Shaughnessy, and A. J. Robinson, "Energy efficiency of electrical infrared heating elements," *Appl. Energy*, vol. 162, pp. 581–588, Jan. 2016, doi: 10.1016/j.apenergy.2015.10.064.

[5] "Flux Mapping of Radiant Electric Heaters Repeatability Considerations, .pdf."

[6] T. Er, H. G. Işık, O. F. Muratoğlu, and A. Karabatak, "Numerical and Experimental Investigations on Radiative Heat Flux Characteristics of an Infrared Quartz Lamp," in *2023 10th International Conference on Recent Advances in Air and Space Technologies (RAST)*, Jun. 2023, pp. 1–6. doi: 10.1109/RAST57548.2023.10197962.

[7] "INDUSTRIAL 13195X/98 1000W 235V - DR. FISCHER EUROPE." Accessed: Mar. 21, 2024. [Online]. Available:https://www.dr-fischer-europe.com/catalogue/ir-en/onde_courte-en/industrielle-13195x-98-1000w-235v/?lang=en.

[8] "Captec Scientific Catalog." Accessed: Mar. 21, 2024. [Online]. Available:http://www.techno-office.com/file/captec-scientific-catalog.pdf.

[9] S. Monteix, F. Schmidt, Y. Le Maoult, R. Ben Yedder, R. W. Diraddo, and D. Laroche, "Experimental study and numerical simulation of preform or sheet exposed to infrared radiative heating," *J. Mater. Process. Technol.*, vol. 119, no. 1, pp. 90–97, Dec. 2001, doi: 10.1016/S0924-0136(01)00882-2.

[10] "13195X/98 1000W 235V REFL Technical Specifications." Accessed: Mar. 21, 2024. [Online]. Available: https://www.sillamps.com/datasheets/PH13195X.pdf.

[11] A. Kunze and B.-E. Ghidersa, "Model-based optimization of the heat flux distribution of IR-heaters for high heat flux testing," *Fusion Eng. Des.*, vol. 124, pp. 215–219, Nov. 2017, doi: 10.1016/j.fusengdes.2017.05.130.

[12] "Radiating Characteristics of Tungsten and Tungsten Lamps." Accessed: Mar. 21, 2024. [Online]. Available: https://opg.optica.org/josa/abstract.cfm?uri=josa-35-2-108.

[13] T. Hoshino, K. Mito, A. Nagashima, and M. Miyata, "Determination of the thermal conductivity of argon and nitrogen over a wide temperature range through data evaluation and shock-tube experiments," *Int. J. Thermophys.*, vol. 7, pp. 647–662, May 1986, doi: 10.1007/BF00502397.